

Functional and Structural Characterization of HIV-1 gp41 Ectodomain Regions in Phospholipid Membranes Suggests that the Fusion-active Conformation Is Extended

Ofir Korazim, Kelly Sackett and Yechiel Shai*

Department of Biological
Chemistry, The Weizmann
Institute of Science, Rehovot
76100 Israel

HIV-1 entry into its host cell involves a sequential interaction whereby gp41 is in direct contact with the plasma membrane. Understanding the effect of membrane composition on the fusion mechanism can shed light on the unsolved phases of this complex mechanism. Here, we studied N36, a peptide derived from the N-heptad-repeat (NHR) of the gp41 ectodomain, its six helix bundle (SHB) forming counterpart C34, together with the N-terminal 70-mer wild-type peptide (N70), and additional gp41 ectodomain-derived peptides in the presence of two membranes, modeling inner and outer leaflets of the plasma membrane. Information on the structure of these peptides, their affinity towards phospholipids and their ability to induce vesicle fusion was gathered by a variety of fluorescence, spectroscopic and microscopy methods. We found that N36, having strong affinity towards phospholipids, prominently shifts conformation from α -helix in an outer leaflet-like zwitterionic membrane to β -sheet in a membrane mimicking the negatively charged inner leaflet environment, leading to pronounced fusion-activity. Real-time atomic force microscopy (AFM) was used to study the peptides' effect on the membrane morphology, revealing severe bilayer perturbation and extensive pore formation. We also found, that the N36/C34 core is destabilized by electronegative, but not zwitterionic phospholipids. Taken together, our data suggest that the fusion-active pore forming conformation of gp41 is extended, upstream of the SHB. In this manner, folding of the ectodomain into a SHB might also serve as a negative regulator of fusion by impeding gp41 fusion-active surfaces, thus preventing irreversible damage to the cell membrane. This assumption is supported by the finding that pre-incubation of large unilamellar vesicles (LUV) with C-heptad repeat (CHR)-derived fusion inhibitors reduces the fusogenic activity of N-terminal peptides in a dose-dependant manner, and suggests that CHR-derived fusion inhibitors inhibit HIV entry in an analogous mechanism.

© 2006 Elsevier Ltd. All rights reserved.

Keywords: membrane fusion; peptide–lipid interaction; HIV-1; FTIR; virus-cell fusion

*Corresponding author

Introduction

The molecular mechanism of fusion between human immunodeficiency virus (HIV) and its host cell has been studied intensely during the past decade, giving rise to a fairly agreed upon working fusion model which is based mostly on inhibitory and structural data. The consecutive initial stages of this interaction are well defined, yet the exact molecular trigger that causes prefused viral and host membranes unification is left obscure.

Abbreviations used: HIV, human immunodeficiency virus; FP, fusion peptide; PC, phosphatidylcholine; PS, phosphatidylserine; NHR, N-heptad repeat; CHR, C-heptad repeat; SHB, six-helix bundle; AFM, atomic force microscopy; LUV, large unilamellar vesicle; SUV, small unilamellar vesicle; FTIR, Fourier transform infrared.

E-mail address of the corresponding author:
Yechiel.Shai@weizmann.ac.il

It has been known that the phospholipid composition of plasma membranes differs between inner and outer leaflets^{1,2} as a result of constitutive enzymatic activity, crucial for cell survival. For example, this lipid asymmetry has been most well characterized in the erythrocyte membrane, of which outer monolayers contain 75–80% of the choline-containing lipids phosphatidylcholine (PC) and sphingomyelin (SM), and no detectable phosphatidylserine (PS). Loss of transmembrane phospholipid asymmetry, with consequent exposure of PS in the external monolayer, occurs in both normal and pathologic conditions. PS externalization is induced early in the process of apoptosis³ and during platelet activation.⁴ The severe forces applied on cell–cell or cell–virus contact areas are enough to cause transient exposure of electronegative phospholipids, such as PS, from the inner leaflet.^{5–7} In the case of HIV entry, such local changes in electro environment are likely to effect the players taking part in this complex process.

HIV entry into its hosting cell is mediated by the envelope glycoproteins gp41 and gp120, non-covalently associated. Surface gp120 is primarily involved in recognition of cellular receptors, whereas gp41 is anchored to the viral membrane and mediates membrane fusion. The gp41 ectodomain contains four distinct functional regions (Figure 1); a Trp-rich pretransmembrane domain (PTD) adjacent the viral membrane, followed by two helical heptad

repeat regions (NHR and CHR) separated by a loop, and a stretch of 15 hydrophobic residues located at its N termini, known as the fusion peptide (FP).

In keeping with the classic sequential fusion model, fusion is initiated by specific binding of gp120 to CD4 cell surface molecules,^{3,8,9} followed by interaction with co-receptors.^{10–12} These interactions, in addition to the reduction of gp120 disulfide bonds mediated by lymphocyte surface-associated protein-disulfide isomerase,¹³ induce major conformational changes in gp120, releasing gp41 from metastable constraints and resulting in its activation.^{14,15} At first, gp41 transiently adopts a trimeric extended prehairpin intermediate (PHI) conformation that bridges both the viral and cellular membranes. The PHI conformation, which is believed to exist for approximately 15 min,¹⁶ is characterized by exposure of the NHR and CHR regions. Collapse of the PHI into a six helix bundle (SHB), whereby three CHR helices pack obliquely in an antiparallel configuration into the highly conserved hydrophobic grooves on the surface of the central NHR coiled-coil,^{17,18} is thought to be the driving force for drawing viral and host membranes into close proximity. It is speculated¹⁹ that once the membranes are pulled together, the contacting monolayer (referred to as *cis*) leaflets merge, but the distal (denoted *trans*) leaflets remain intact. This intermediate structure later evolves to form a hemi-fusion diaphragm. The *trans*-monolayers making up

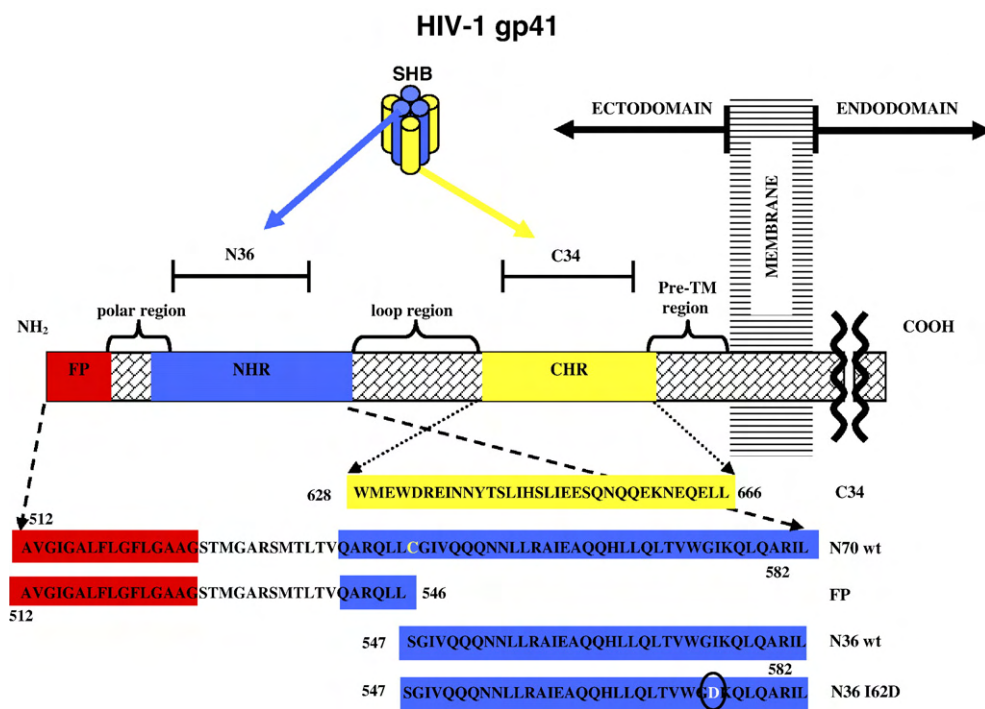


Figure 1. Scheme of the HIV-1 gp41 primary structure. Primary functional regions are colored and outlined with additionally characterized regions specified above by a brace. Above the gp41 structure, the N36/C34 helix bundle, composed of three C34 helices (yellow) from the C-peptide region packed obliquely in an antiparallel configuration into the highly conserved hydrophobic grooves on the surface of the central N36 (blue) coiled-coil is illustrated. Below are the peptides represented in this study, which are derived from the indicated N and C-terminal subdomains. The residues are numbered according to their position in gp160.

the hemifusion diaphragm then rupture to form the complete fusion pore.²⁰ Peptides derived from the NHR and CHR regions of gp41 were found to inhibit HIV-1 fusion,^{21,22} presumably by binding their endogenous counterparts, leading to inhibition of SHB formation, which results in arrestment of the fusion process. One of these peptides, DP178,²³ which is a C-terminally extended CHR, was recently approved by the FDA and is currently part of HIV-1 treatment.

There are mounting findings that question this sequential model, specifically examining the role of SHB formation in the events prior to fusion. Various peptide segments of the gp41 ectodomain such as the fusion peptide,²⁴ an extended FP,^{25,26} a peptide pertaining to the loop segment separating the NHR from the CHR,²⁷ and the 20-mer PTM²⁸ were found to have intrinsic fusogenic activities on model membranes. The way these segments cause membrane unification and pore formation in the context of the whole ectodomain is unclear. It has been shown, that the C-terminal subdomain specifically destabilizes the virion-like cholesterol-rich membrane, whereas the N-terminal subdomain is more effective in fusing target-like, unordered membranes containing lower amounts of cholesterol.²⁹ Regarding the fusion sequence, it was demonstrated that pores are formed before the folding of Env into bundles is complete³⁰ and that the binding of NC-1, a monoclonal antibody specific for N-helical gp41 trimers, reaches its maximum 10 min after initiation of a fusion reaction, but before dye transfer between cells occurs³¹ (matching the time the PHI conformation is believed to exist¹⁶), followed by a rapid decrease. Although this reduction in antibody signal might arise from steric hindrance of fusion machinery,³² it also could result from the destabilization of the rigid SHB structure during the process of fusion as previously offered by Kliger *et al.*³³ and Dimitrov *et al.*³¹ Kliger *et al.*³³ showed that the N36/C34 core is destabilized in negatively charged membranes, but its role in zwitterionic membranes was not investigated.

Here, we studied various N-terminal regions of gp41 in the presence of two membranes, modeling inner and outer leaflets of the plasma membrane. Information on the structure of these peptides, their affinity towards phospholipids, and their ability to induce vesicle fusion and pore formation was gathered by using fluorescence, FTIR, electron microscopy, and atomic force microscopy (AFM). Our results indicate that the NHR undergoes a structural shift from an α -helix to a β -sheet structure upon interaction with electronegative membranes, leading to pronounced fusion-activity and pore formation. Interestingly, this fusion activity is inhibited by CHR-derived peptides. Moreover, we found that the N36/C34 core is destabilized by electronegative, but not zwitterionic phospholipids. We discuss our results in relation to the current gp41 fusion model, and to an additional mode of action by which CHR-derived fusion inhibitors restrain HIV entry.

Results

Six peptides derived from the gp41 ectodomain (Figure 1) were synthesized and studied in the presence of two model membranes, mimicking the inner and outer leaflet plasma membranes. The peptides include N36 and C34, which form a six helix bundle when mixed in a 1:1 molar ratio, N36 (I62D) mutant,³⁴ the N terminal 34-mer hydrophobic FP, N70, a construct comprising both FP and N36, and the fusion inhibitor DP178. N70 has recently been shown to adopt a native trimeric oligomeric state in solution, detected by its ability to bind the trimeric N-helical specific monoclonal antibody NC-1.⁶⁷ The outer leaflet zwitterionic membrane was modeled by PC:cholesterol (9:1) whereas the inner leaflet negatively charged face was modeled by PC:PS:cholesterol (4.5:4.5:1).

The NHR region (residues 547–582) fuses negatively charged phospholipids

The comparative fusion-activity of N36, its I62D mutant, 34-mer FP and the N70 construct on PC:PS negatively charged vesicles (Figure 2(a)) indicates

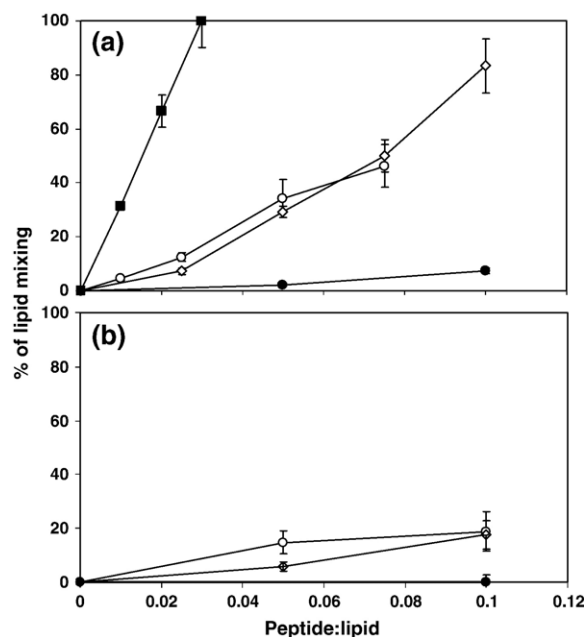


Figure 2. Dose-dependant lipid mixing of PS containing LUV induced by gp41 ectodomain peptides. Peptide aliquots were added to mixtures of LUV (110 μ M phospholipids concentration) containing 4.5:4.5:1 (a) or 8.5:0.5:1 (b) PC:PS:cholesterol LUV prelabeled with 0.6 mol % NBD-PE and Rho-PE in PBS (pH 7.4) buffer. Increase of NBD-PE fluorescence intensity was measured 10 min after the addition of the peptide, and the percentage from the maximum (referred to 0.03 peptide/lipid N70 in (a) or 10 μ l Triton in (b)) is plotted *versus* the peptide/lipid molar ratio. The experiments were repeated at least twice with the error bars for each point reflecting the total variation. Symbols: (■) N70, (○) N36; (●) N36m, and (◇) FP.

that N36 has a significant fusion-activity, similar to the FP, used here as a positive control.^{24,35} N36 activity is phospholipid-dependant as decreasing the relative amount of PS to 5% reduces the peptide's activity significantly (Figure 2(b)). In a completely zwitterionic environment N36 possesses negligible fusogenic capabilities (data not shown). N70 is roughly four times more fusogenic than its deconstructed components (FP and N36), in accordance with our previous findings using similar fragments on PC membranes.²⁶ However, in contrast with the high fusogenic activity of N36 on PC:PS found here, it was not active on PC membranes.²⁶ A single mutation in the N36 sequence, known to be lethal *in vivo*³⁶ and to disrupt its helical structure in NHR fragments,³⁴ causes a substantial loss of function on these membranes. Note that a recent study done with a shorter NHR-derived peptide partially overlapping N36 (residues 568–588 of the HXB2 strain)³⁷ shows that the peptide induces leakage and mixture of different homogenous membranes.

To confirm the fusion-activity of the NHR-derived segment, we compared the interaction of N36 and its I62D mutant with PC:PS:chol membranes by using transmission electron microscopy (Figure 3). The EM images verify that addition of N36 causes notable vesicle enlargement compared to the untreated control image ($p < 0.0007$), whereas N36 (I62D)m does not affect the mean vesicle diameter significantly ($p < 0.4$).

Real-time AFM exhibits severe nanoscale holes in electronegative membranes induced by gp41 N-terminal segments

Topographic images obtained for PC:PS:chol (4.5:4.5:1) bilayers in 30 mM NaCl with or without 10% DMSO, reveal a single phase, continuous membrane layer, scarcely dotted with round defects of $80(\pm 25)$ nm diameter, 5 nm deep (Figure 4, upper row). Incubation of the same bilayer region with three gp41 ectodomain peptide solutions (6 μ M) for ~ 10 min altered the membrane morphology prominently and distinctively as seen in Figure 4, second row. FP induced a homogeneous distribution of $5(\pm 1)$ nm deep holes with a diameter of ~ 200 nm, while unaffected the global shape of the bilayer surface. N36, unlike the FP, did not induce distinctive pores, but rather had a global effect on membrane morphology. Phospholipids were unevenly distributed immediately after addition of a peptide, forming oscillations in membrane height, scattered ~ 300 nm from each other throughout the sample. Supramolecular assemblies or precipitates were not seen before addition of the peptide to the bilayer surface. Our understanding of the mechanism by which the peptide induces this morphology is limited, and further experiments are needed to understand the details of the peptide-lipid complex. Similar morphological changes in membranes caused by other amphipathic model peptides have been reported,³⁸ bringing us to hypothesize that two

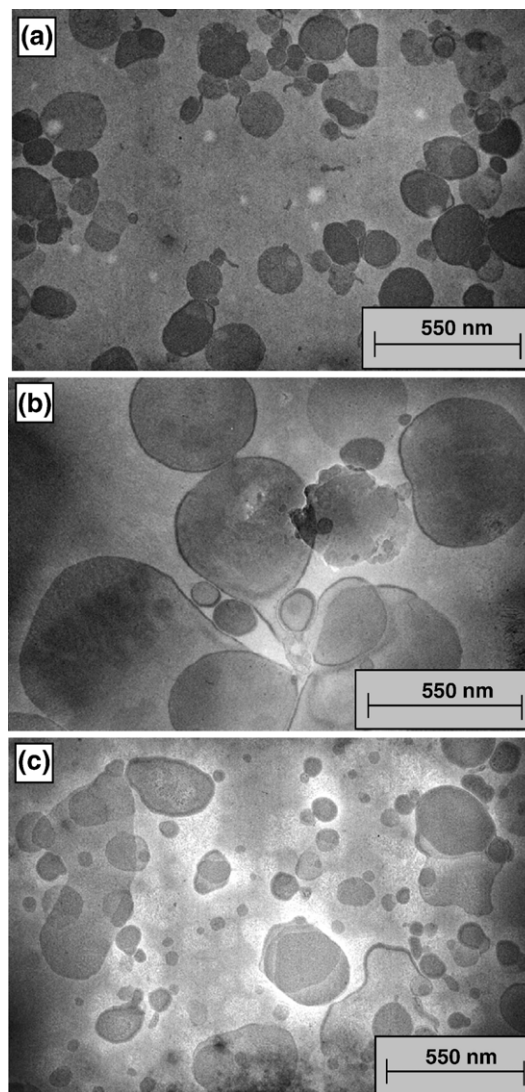


Figure 3. Electron micrographs. Shown are micrographs of negatively stained 4 mM PC:PS:cholesterol (4.5:4.5:1) LUV in the absence and presence of two different peptides at 0.1 peptide/lipid molar ratio. (a) PC:PS:chol LUV; (b) PC:PS:chol LUV incubated with N36; (c) PC:PS:chol LUV incubated with N36m.

factors are involved in phospholipids rearrangement; the amphipathic nature of N36 and the negative charge of the serine head groups. The peptide's hydrophobic face is attracted to the lipids' fatty tail, while the hydrophilic, positive face, is concurrently attracted to the electronegative head groups, thereby forming discrete peptide-lipid complexes. N70, possessing both FP and N36 perturbation capabilities, shows a synergistic activity of the two; it induces massive pore formation (~ 200 nm between pores, $5.5(\pm 1.5)$ nm deep holes), accompanied by larger scale oscillations in membrane height. These findings indicate that the 70-mer N terminus of gp41 is capable of inducing fusion pores in negatively charged membranes. In light of the clear functional correlation between lipid mixing and AFM findings, we searched for a

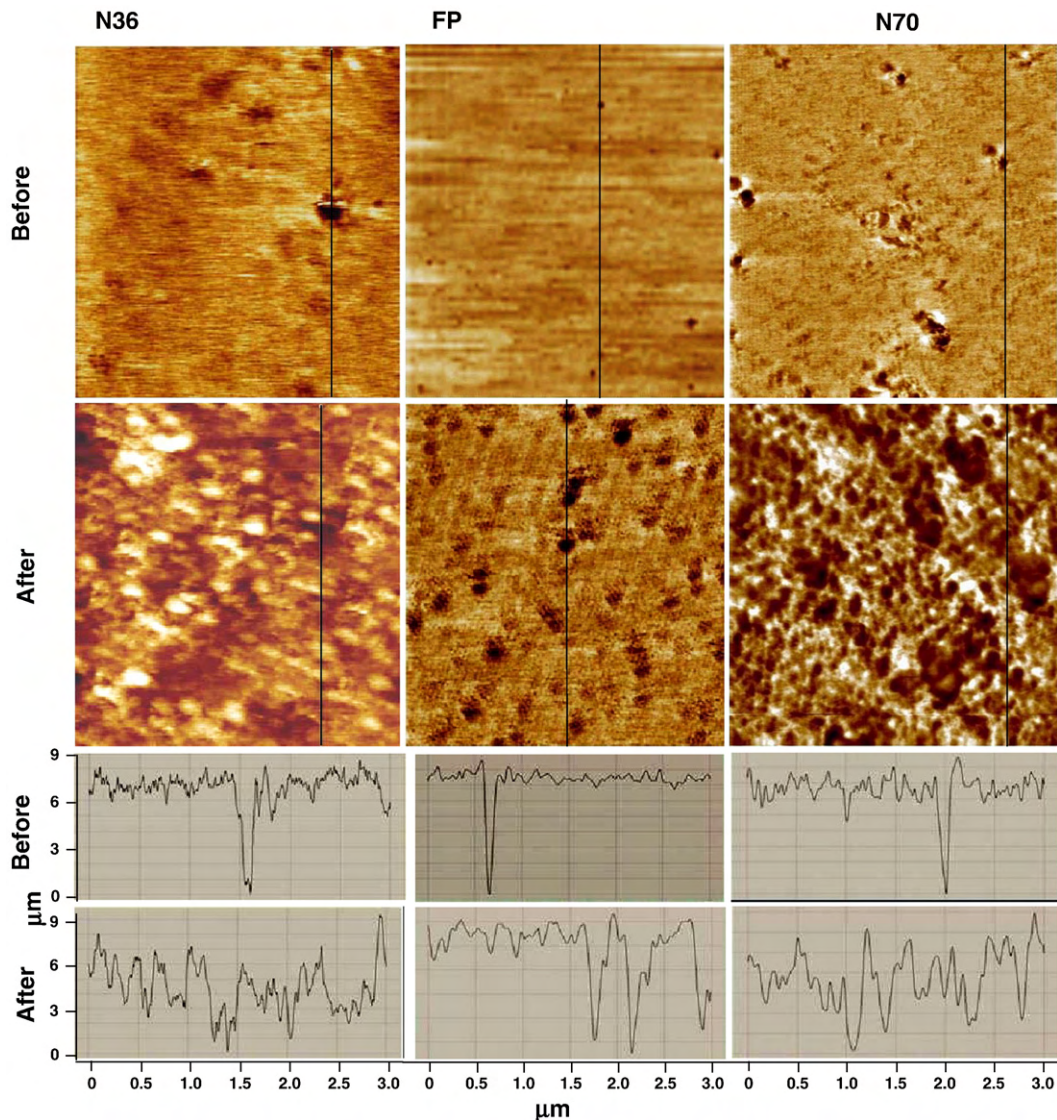


Figure 4. Real-time AFM images ($3\ \mu\text{m} \times 3\ \mu\text{m}$; z scale, 9 nm) of the effect caused by three ectodomain peptides. The interaction between N36 (left), FP (middle) and N70 (right) with PC:PS:chol (4.5:4.5:1) supported lipid membranes has been imaged in real-time, in aqueous buffer with AFM. Lipid bilayers were scanned before (upper row) and ~ 10 min after (second row) addition of $6\ \mu\text{M}$ peptide solution. Matching cross-sections for the above images taken along the black lines ($3\ \mu\text{m}$; z scale, 9 nm) are presented at the bottom two rows.

structural link in electronegative membranes using FTIR.

The NHR secondary structure is shifted from α -helical in an outer-leaflet-zwitterionic membrane to β -sheet in an inner-leaflet-negatively charged one

FTIR spectroscopy was used to ascertain changes in secondary structure elements of the peptides caused by incorporation into the two membranes mimicking inner and outer plasma membrane leaflets. In the amide I region, different secondary structure components can be characterized by resolvable vibrational frequencies. In order to best resolve between helical and disordered structures which overlap, we analyzed the IR spectra of membrane-associated peptides following complete

deuteration. The positions of the component bands in the amide I spectra were identified as peaks in the second derivative. These wavelengths were used as initial parameters for curve fitting with Gaussian component peaks. The FTIR spectra for each peptide in the different environments, together with the assignments, wavelengths, and relative areas of the component peaks are summarized in Figure 5 and in Table 1. Notably, N36 shows a distinctive conformational shift from 29% β -sheet in an outer leaflet-like zwitterionic membrane to 84% in a membrane mimicking the inner leaflet negatively charged membrane. The N36(I62D)_m peptide gives a similar, yet slightly moderated environment-dependent conformational shift (from 32% to 70%). Regarding the FP, our results verify distinctive β -sheet structure in zwitterionic membranes,³⁹ and show that it maintains this conformation in a negatively charged

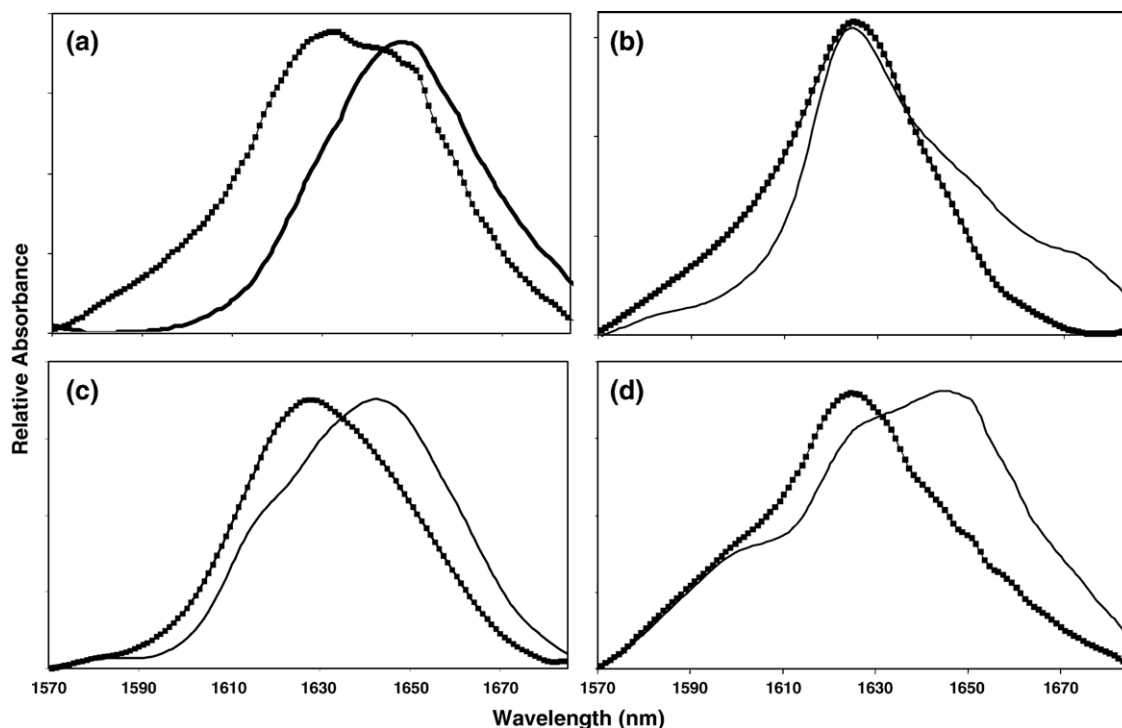


Figure 5. Membrane-dependant conformational shift of N36. ATR-FTIR spectra of fully deuterated amide I bands ($1570\text{--}1685\text{ cm}^{-1}$) of the four ectodomain peptides in zwitterionic (continuous, thin) and PC:PS:cholesterol electronegative (broken, thick) membranes. Peptides N36, FP, N36m and N70 are represented by (a), (b), (c), and (d) respectively.

environment. N70, which shares both helical and β -sheet contributions from the NHR and FP respectively, shows a significant increase in its β -sheet structure in a negatively charged milieu, most likely originating from the NHR conformational shift. An unknown peak corresponding to the boundary of the amide I band (1600 cm^{-1}) had similar contributions to the N70 FTIR spectra at both membrane environments.

N36 and N36(I62D)m bind zwitterionic and negatively charged phospholipids with similar affinities

We used the sensitivity of tryptophan fluorescence to the polarity of its environment⁴⁰ to

detect membrane binding as described in Materials and Methods. An increase of Trp fluorescence concomitant with a blue shift was observed upon addition of SUV to the peptides' solution (Figure 6), suggesting that both peptides bind to the membrane. The calculated surface partition coefficient of N36 is $(1.2 \pm 0.2) \times 10^4$ for the PC:chol, and similarly $(1.3 \pm 0.1) \times 10^4$ for PC:PS:chol. The value obtained with PC:PS:chol using the intrinsic Trp fluorescence, is in agreement with results obtained previously by using extrinsic fluorescently labeled N36 in PC/PS.³³ The mutant peptide, although non-fusogenic, shares a similar partition coefficient in zwitterionic membranes as the wild-type $((1.1 \pm 0.1) \times 10^4)$, and it binds slightly less negatively charged lipids $((0.7 \pm 0.1) \times 10^4)$.

Table 1. Secondary structure content of the peptides determined by ATR-FTIR spectroscopy

Peptide	Random 1640–1646	α -Helix 1648–1655	β -Sheet 1620–1640	3_{10} Helix 1655–1670	β Turn 1670–1680	Others 1590–1620
<i>PC Phospholipids</i>						
N36		1649 (53%)	1631 (29%)	1669 (18%)		
N36m	1642 (49%)		1621 (32%)	1659 (19%)		
FP	1646 (24%)		1626 (65%)		1670 (11%)	
N70		1649 (53%)	1624 (28%)		1676 (4%)	1600 (15%)
<i>PS Phospholipids</i>						
N36		1649 (12%)	1630 (84%)	1666 (<5%)		
N36m		1648 (30%)	1625 (70%)			
FP	1644 (34%)		1626 (50%)	1656 (<5%)		1593 (12%)
N70		1648 (25%)	1625 (52%)			1600 (23%)

The wave number of each component peak after deconvolution is indicated, with the percent area relative to the sum of contributing component peaks in parenthesis.

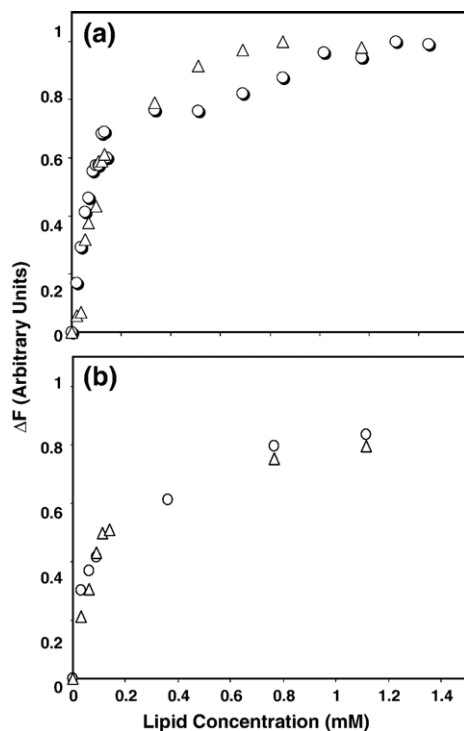


Figure 6. Membrane binding isotherms of N36 and N36m. Changes in the intrinsic tryptophan fluorescence intensity of N36(Δ) and N36m(\circ) when titrated with PC:chol (a) or PC:PS:chol (b) membranes. K_a values derived from the charts show minor differences in the peptides' affinity towards both membranes (c).

This minor difference cannot account for the distinct abilities of the two peptides to fuse negatively charged membranes.

N36/C34 core is protease-resistant in solution

To study effects of pre-formed cores in membranes, we followed changes in fluorescence of labeled peptides either free or complexed in cores, both in solution and upon interaction with membrane vesicles. The fluorescence of the rhodamine probe is quenched upon close association (for example, upon core formation between peptides, or aggregation of free peptide), and increases as the average distance between rhodamine moieties increases (for example, upon core dissolution or digestion by protease). Resistance to proteolytic digestion was monitored to gauge core integrity in solution and to follow membrane interaction.

Figure 7 summarizes the results obtained with free Rho-C34 (a), Rho-C34 within the core (b), free Rho-N36 (c), and Rho-N36 within the core (d). Comparing red lines (peptides in solution) in Figure 7(a) and (b), we see that the fluorescence of free Rho-C34 (Figure 7(a)) is initially high and sharply increases within 20–30 s upon digestion with protease (point 1), indicating that Rho-C34 exists partially as weakly bound oligomers. In comparison, in the context of the core (Figure 7

(b)), Rho-C34 is also digested but with a slow kinetics, confirming N36/Rho-C34 protease resistance in solution. The stability of the core in solution was also confirmed when using Rho-N36. Comparing red lines in Figure 7(c) and (d), we see that the fluorescence of free Rho-N36 (Figure 7(c)) is initially very low and digested more slowly in solution than its corresponding core, Rho-N36/C34 (Figure 7(d)). This attests to the fact that N36 highly aggregates in solution, thereby shielding it from protease access,⁴¹ whereas its trimeric organization in context of the N36/C34 core presents a partially exposed N terminus. Although free N36 is initially digested more slowly than its corresponding core, it is fully digested within 2 h, while the core retains a measure of protease resistance.

N36/C34 core destabilizes in electronegative, but not in zwitterionic membranes

Figure 7(d) reveals that Rho-N36/C34 core dissociates rapidly when PC:PS vesicles (blue line, point 1) are added, but unexpectedly does not appreciably separate when PC vesicles (black line, point 1) are introduced. The kinetics and extent of protease digestion (point 2) in PC membranes are similar to digestion in solution, showing that the Rho-N36/C34 core is preserved in PC. When the Rho-label was placed in C34 (Figure 7(b)), we see that the core does not dissolve appreciably in the presence of either PC (black line, point 1) or PC:PS (blue line, point 1) membranes. However, upon addition of protease (point 2) to cores in membranes, the N36/Rho-C34 core is digested rapidly after interaction with PC:PS, indicating that the complex unfolds in PC:PS, exposing free Rho-C34 to protease. The same core in PC membranes follows digestion kinetics as if it was in solution alone, indicating the core does not open in PC.

The fact that the N36/C34 core behaves differently in electronegative PC:PS membranes depending on which peptide constituent carries the probe, is a function of the behavior of the free peptides themselves in the different membranes. Incubation of Rho-N36 in membranes shows near complete dissolution of the large aggregates in PC:PS (blue line) within 2 h, with only partial dissolution in PC in the same time frame. An electrostatic effect is plausible, since N36 carries a net positive charge of +3 at physiologic pH. In contrast, Rho-C34 exists as weakly bound oligomers in both PC:PS and PC membranes, but rapidly digested in both membranes upon the addition of protease. Though we have shown previously that the N36/C34 core destabilizes in electronegative PC:PS vesicles,³³ our current study shows that membrane phospholipid composition is a key determinant of core stability in membranes, with zwitterionic PC membranes supporting quaternary complex stability of interacting cores. Based on detailed fluorescence analysis of N36/C34 cores and their component free peptides, we conclude that under physiologic conditions, the N36/C34 core is preserved upon interaction with

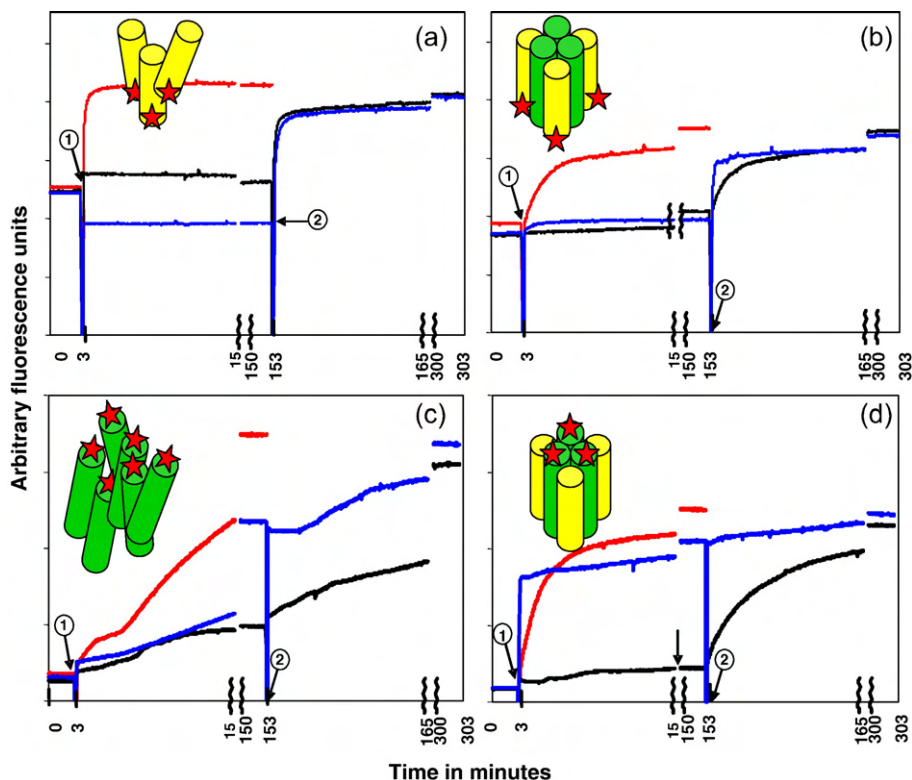


Figure 7. The effect of membrane binding on the N36/C34 core. Free Rho-labeled peptide (Rho-C34 in (a), and Rho-N36 in (c), 0.5 μM each) or pre-formed cores with the corresponding Rho-labeled peptides ((b) and (d), respectively) were equilibrated overnight in solution at room temperature in stirred glass cuvettes. After 3 min measurement of fluorescence intensity (point 1), either protease K (62.5 $\mu\text{g}/\text{ml}$ final concentration, red line) or vesicles (900 μM final concentration of PC (black line) or PC:PS (blue line)) were added and data collected for additional 15 min. Following an additional 2.5 h incubation at room temperature in the dark, proteinase K (62.5 $\mu\text{g}/\text{ml}$ final concentration) was added (point 2) to all samples in membranes, with an additional 15 min kinetic measurement. Following 2.5 h incubation, equilibrium measurements were recorded for additional 3 min. All measurements were done in PBS (pH 7.4). Pre-formed cores were prepared with Rho-peptide (0.5 μM) and excess of unlabeled counterpart peptide (1 μM). Red star denotes rhodamine.

zwitterionic PC membranes, but destabilizes in electronegative PC:PS membranes.

CHR-derived fusion inhibitors reduce the fusogenic activity of N-terminal peptides in a dose-dependant manner

Pre-mixing of negatively charged LUVs with C34, known to potentially inhibit gp41-mediated fusion *in vitro*³⁸ and *in vivo*,⁴¹ reduces the extent of fusion caused by gp41 N-terminal peptides significantly (Figure 8). N36 is clearly affected, showing dose-dependant inhibition (>50% inhibition at [1:3] N36:C34 molar ratio). This inhibitory activity of C34 on N36 is likely to arise from two, independent interactions: (i) the highly thermostable hydrophobic interaction between C34 and N36, shielding the active membrane perturbing surfaces of N36; (ii) the medium affinity interaction between C34 and the negatively charged LUVs ($\Delta G = -7.1$ kcal/mol^{5,33}), shielding the membrane from binding by N36. C34 and N36 are likely to interact and oligomerize both in solution and on the LUVs, preventing the conformational change of N36 into β -sheet, thereby reducing its fusogenic capability. C34 inhibitory

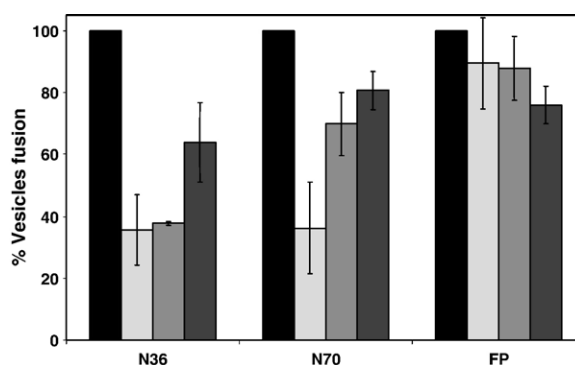


Figure 8. The inhibitory effect of C34 on the fusogenic activity of the N-terminal peptides. Varying concentrations of the CHR-derived C34 peptide (left to right 0, 22, 8, 4.5 μM), incapable of inducing vesicle fusion, were pre-incubated with PC:PS:chol (4.5:4.5:1) LUVs until equilibration. Then, the 8.25 μM (or 3.3 μM in the case of N70) fusogenic N-terminal peptides N36, N70 or FP were added to the peptide-lipid mixture and equilibrated. 100% mixing refers to the fusogenic activity of each peptide in the absence of inhibitors. Colors: black, no inhibitor; light gray, (3:1) C34:peptide; medium gray, (1:1) C34: peptide; dark gray, (2:3) C34:peptide.

effect on N70 is similar to its effect on N36 both qualitatively and quantitatively. Since N70 comprises both FP and N36, and since the inhibitory effect of C34 on N36 is approximately two orders of magnitude stronger than its effect on the FP, we deduce that N70 inhibition by C34 is governed primarily by the CHR–NHR interaction. The fusogenic activity of the FP, which has not been shown to directly interact with C34, is also slightly reduced by C34 pre-incubation. The basal inhibition of FP, which does not show dose dependency, may result from the effect of C34 on the physical properties of the LUV similarly to what has been shown with other class A amphipathic helices.⁴² Last, the HIV entry inhibitor DP178 (*fuzeon*TM), which is shifted ten residues C-terminally relative to C34, has a ~10% reduced inhibitory effect on N70 compared to C34 (data not shown). This could result from the non-overlapping residues (628–638) present in C34 but not in DP178, shown to form a large cavity when bound to residues 566–576 in N36.¹⁷

Discussion

Here, we show that interactions between gp41 ectodomain segments and model membranes are affected by changes in the phospholipid composition of the membranes. Our results indicate that the NHR shifts conformation to β -sheet in an electronegative environment (Figure 5), enhancing its fusion-activity exceedingly (Figures 2 and 3), and that synergistically with the FP it induces formation of fusion pores in this environment (Figure 4). This activity can be inhibited by CHR-derived peptides that shield the membrane perturbing surfaces of N36 (Figure 8). Taken together, these results point out that the fusion-active conformation of gp41 is extended, upstream of the SHB.

To date, the main function of the NHR in the context of fusion is to stabilize the trimeric oligomeric state of the gp41 ectodomain, forming a central coiled coil at the PHI stage, crucial for increasing the FP's ability to fuse membranes.^{26,43} Our results show that in addition to this function, the NHR takes an active role in destabilizing membranes enriched in electronegative phospholipids, which may occur locally in the process of viral fusion due to the membrane perturbing effect of the FP. In support of this it has been shown that the severe forces applied on cell–cell or cell–virus contact areas cause transient exposure of electronegative phospholipids, such as PS, from the inner leaflet.^{5–7}

Structural characterization of the discrete FP has revealed seemingly paradoxical data; α -helix or β -structure,^{25,44–48} yet under NHR stabilization in the context of N70, the FP has been shown to adopt parallel β -sheet structure in zwitterionic membranes.³⁹ Moreover, there is a direct correlation between FP β -structure and fusogenic function.⁴⁹ Here, the infrared spectrum of the FP in the presence of electronegative membranes shows that it main-

tains β -structure regardless of electrostatic environment (Figure 5). Surprisingly, N36 shows a distinct shift toward β -structure upon exposure to electronegative phospholipids, an alteration that is also reflected in the spectra of N70. The latter's structure is predominant β -sheet in an electronegative environment, which may explain its extensive ability to fuse and induce formation of pores in these membranes. Figure 7(c) suggests that N36 forms oligomers, prior and when bound to membranes, because the fluorescence of Rho-N36 is quenched when bound to PS:PC membrane (Figure 7(c), blue line, point 1), but gradually increases after the addition of proteinase-K to the membrane-bound peptide (point 2). The extended β -structure of the N-terminal half of gp41's ectodomain would also favor aggregation of trimers during the PHI stage, a mechanism that could markedly induce pore formation, analogously to the proposed mechanism of ion channel formation in the case of many amyloid diseases.^{50–52}

The NHR's ability to bind phospholipids is inadequate to account for its fusogenic quality, as an isoleucine to aspartic acid mutation known to cause structural destabilization³⁴ does not abolish the peptide's ability to bind membranes irrespective of their charge (Figure 6), yet it abolishes function completely. Structural differences between N36 and its I62D mutant are also insufficient to explain the discrepancies in fusion-activity. Although the peptides differ structurally in zwitterionic milieu, they adopt similar conformations in electronegative, fusion-active environment (Figure 5). The cause for their distinct activities in electronegative membranes is therefore left to be further investigated.

Identification of the sequential events that take place subsequent to gp41 activation and leading to pore formation have been brought to the front of HIV fusion research since the crystal structure of the gp41 core was revealed.¹⁷ According to the predominant thought, SHB formation occurs prior to pore formation and is therefore essential for its initiation. It is based on the findings that: (1) ectodomains of many viral fusion proteins fold into bundles when in solution; (2) peptides that block bundle formation prevent fusion;^{53,54} (3) mutations in gp41 that abolish infectivity and fusion often map to residues within the heptad repeats that are expected to stabilize the SHB^{36,55–58}. Yet none of these studies propose that these mutations might harm the intrinsic fusogenic activity of the extended gp41 conformation, nor do they provide direct experimental evidence that SHB formation is a prerequisite for pore formation. Moreover, the mAb NC-1 raised against the SHB binds the exposed surface of the trimeric NHR coiled coil.³¹ The first to challenge the idea that SHB formation is prerequisite for fusion were Markosyan *et al.*,³⁰ who used a temperature jump technique to show that pores are formed before the folding of gp41 into bundles is complete. Later, Dimitrov *et al.*³¹ who monitored temporal conformational states of gp41 by using various monoclonal antibodies, concluded that two

parallel pathways of gp41 conformational rearrangements co-exist: one leading to SHB formation and the other leading to generation of gp41 monomers. Our findings provide reinforcing evidence for this notion, and in addition suggest a revision to the final steps of the gp41 fusion model.

As gp41 is released from metastable constraints, the N-terminal FP is thought to be inserted into the target membrane, although no direct verification is available for this state. Interaction of free FP fragments with membranes was known to cause local membrane perturbation in cells⁵⁹ or fusion of liposomes in biophysical assays.^{24,26,35} Here, we show that it is also capable of inducing the formation of pores in an electronegative, inner-leaflet-like membrane. Such disturbance is likely to be sufficient for inducing transient, local exposure of electronegative phospholipids to the outer leaflet, as it has been shown that the forces acting at the contact surfaces of cell–cell^{5,6} or cell–virus,⁷ interactions that lead to fusion, cause exposure of PS. In the case of HIV, we deduce that transient exposure of electronegative phospholipids caused by FP insertion into the target membrane at the PHI configuration is sufficient to trigger NHR fusion-activity. This assumption is based on our findings that: (1) N36 is sensitive to changes in the electro-environment, as it increasingly gains fusogenic capabilities when exposed to escalating levels of electronegative membranes (Figure 2), so that in a highly electronegative environment its ability to fuse liposomes is similar to that of the FP in the same environment; (2) N36 shifts its secondary structure from α -helical in a zwitterionic environment to β -sheet in an electronegative surrounding (Figure 5); (3) The NHR has a strong affinity towards membranes, regardless of their charge (Figure 6). Once triggered by the presence of electronegative head groups, the whole segment of gp41 N-terminal to the CHR (residues 512 to 613), including the FP, NHR and the loop²⁷ separating NHR from CHR, becomes an active fusion driver. This extended segment is likely to induce pore formation and maintain excessive fusogenic capabilities as demonstrated by our AFM images, whereby gp41 N-terminal peptides generate severe damage and form nanoscale pores in an electronegative model membrane (Figure 4). This destructive activity is likely to persist until the gradual antiparallel packing of the SHB, or alternatively, by binding CHR-derived fusion inhibitors such as DP178 and C34. The inhibitory effect of such peptides on N36 and N70 suggests that they inhibit gp41-mediated fusion by concealing the unpacked, fusion driving faces of the ectodomain rather than, or in addition to, preventing SHB formation. The fact that the N36/C34 core is destabilized by electronegative, but not zwitterionic phospholipids, supports this scheme and implies that inner leaflet phospholipids may serve as a positive regulator of fusion by controlling the kinetics of ectodomain folding into a SHB. This inhibitory effect would prolong the time of PHI existence, ensuring pore formation and enlargement. Figure 9 shows a cartoon of the proposed model,

which is a modification of the model proposed by Dimitrov *et al.*³¹ In both models populations of the exposed pre-hairpin conformation co-exist with the SHB. Therefore, membrane apposition induced in the course of SHB formation assists the extended pre-hairpin to exert its pore formation and fusogenic activities. Inhibition of fusion by synthetic CHR can be achieved by inhibiting the formation of the SHB, which prevents membrane apposition, and/or alternatively by directly binding the NHR and inhibiting its fusogenic activity.

To summarize, our results indicate that the fusion-active, pore-forming conformation of gp41 is extended upstream of the SHB, and that folding into a SHB, restrained by electronegative phospholipids, impedes the exposed fusion-active surfaces of the ectodomain.

Materials and Methods

Materials

Rink amide MBHA resin and 9-fluorenylmethoxycarbonyl (Fmoc) amino acids were purchased from Calbiochem-Novabiochem AG (Switzerland). Other reagents used for peptide synthesis included trifluoroacetic acid (TFA, Sigma), *N,N*-diisopropylethylamine (DIEA, Aldrich), methylene chloride (peptide synthesis grade, Biolab, IL), dimethylformamide (peptide synthesis grade, Biolab, IL), and benzotriazolyl-noxy-tris (dimethylamino) phosphonium-hexafluorophosphate (BOP, Sigma). Egg PC and egg bovine brain PS were purchased from Lipid Products (South Nutfield, UK). *N*-(Lissamine rhodamine B-sulfonyl) dioleoylphosphatidylethanolamine (Rho-PE) and *N*-(7-nitrobenz-2-oxa-1,3-diazol-4-yl) dioleoylphosphatidylethanolamine (NBD-PE) were purchased from Molecular Probes (Eugene, OR). Cholesterol (extra pure) was supplied by Merck (Darmstadt, Germany).

Peptide synthesis

The N36, N36(I62D)m, FP, and C34 were synthesized manually on Rink Amide MBHA resin by using the Fmoc strategy as described.^{60,61} They were cleaved from the resin using a cocktail made of TFA:DDW:TES:thioanisole:EDT (44.4:2.3:1:1:1.25 (by vol.)). The 70 residue peptide (N70) was synthesized in two pieces and then ligated chemically as described.⁴³ N-terminal peptide labeling was carried out as described.⁶² All the peptides were purified by reverse phase high performance liquid chromatography (RP-HPLC) on a column to >98% homogeneity and lyophilized. The peptide composition and molecular mass were confirmed by platform LCA electrospray mass spectrometry and amino acid analysis.

Preparation of large (LUV) and small unilamellar vesicles (SUV)

Thin films of PC:cholesterol (9:1) or PC: PS:cholesterol (8:1:1 or 4.5:4.5:1) were generated following dissolution of the lipids in a 2:1 (v/v) mixture of CHCl₃/MeOH and then dried under a stream of nitrogen gas while rotating. Two populations of films were generated: (1) lipid only mixtures, termed unlabeled and (2) the same lipid mixture containing 0.6% molar of NBD-PE and RHO-PE each, termed labeled. The films were lyophilized overnight,

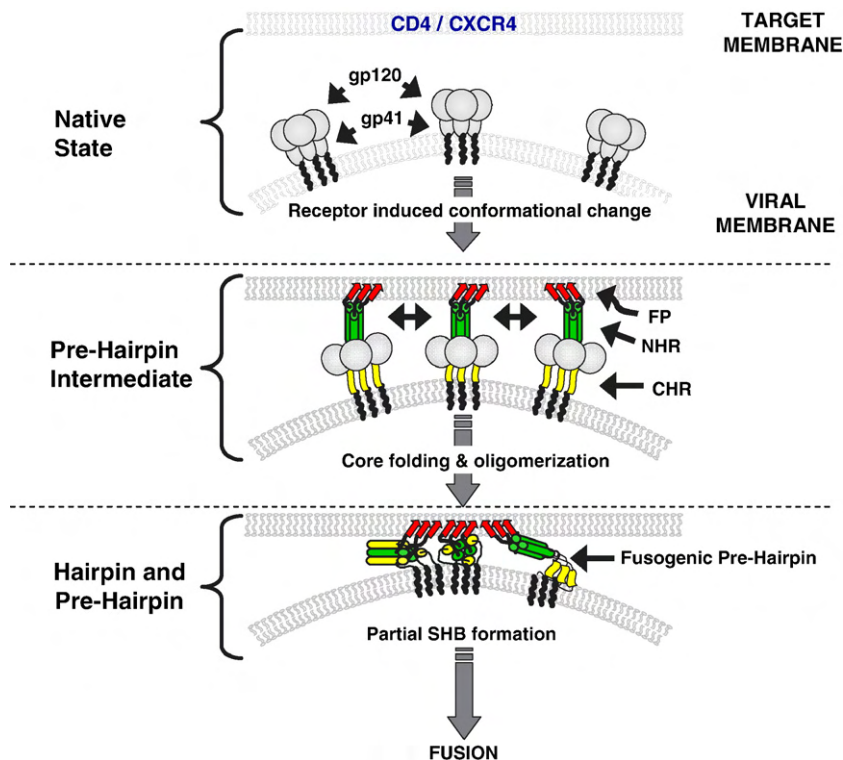


Figure 9. The HIV fusion model. Gp41 is held in a metastable conformation by gp120 in the native state. The interactions of HIV-1 gp41 trimers with CD4 clusters induce conformational changes that result in the exposure of the binding site on gp120 that can engage CXCR4 and the exposure of the gp41 prehairpin intermediate trimer in the target membrane. This is followed by engagement of CXCR4 clusters complex that results in six-helix bundle formation to a fraction of the complex. The remaining exposed pre-hairpin conformation exposed on the surface of the target membrane and susceptible to NC-1 MAb binding,³¹ can initiate pore formation and fusion. Inhibition of fusion by synthetic CHR can be achieved by inhibiting the formation of the SHB, which prevents membrane apposition, and/or alternatively by directly binding the NHR and inhibiting its fusogenic activity.

sealed with argon gas to prevent oxidation, and stored at -20°C . Before the experiment, the films were suspended in the appropriate buffer and vortexed for 1.5 min. The lipid suspension underwent three cycles of freezing-thawing and then extrusion through polycarbonate membranes with $1\ \mu\text{m}$ and $0.2\ \mu\text{m}$ diameter pores to create LUVs as envisioned by electron microscopy. In order to prepare the SUVs, unlabeled films were dissolved in the appropriate buffer, vortexed for 1.5 min, sonicated until clear, and further diluted.

Fluorescence spectroscopy

All fluorescence measurements were performed on a SLM-AMINCO Bowman series 2-luminescence spectrometer at room temperature. Typical spectral bandwidths were $8\ \text{nm}$ for excitation and $8\ \text{nm}$ for emission. The sample was placed in $5\ \text{mm} \times 5\ \text{mm}$ quartz cuvettes with constant magnetic stirring. The data were corrected for background intensities and progressive dilution.

Lipid mixing

Lipid mixing of LUVs was measured using a fluorescence-probe dilution assay.⁶³ LUVs were prepared with PBS CaCl_2 MgCl_2 depleted buffer (PBS, pH 7.4) as described above from a mixture of unlabeled and labeled films at a 9:1 ratio of $110\ \mu\text{M}$ total lipid concentration. Basal fluorescence level was measured initially for $400\ \mu\text{l}$ vesicle mixture. Then, peptide dissolved in a maximum volume of $10\ \mu\text{l}$ dimethyl sulfoxide (DMSO with $5\ \text{mM}$ DTT), was added. Fluorescence was monitored for 10 min after addition of the peptide, to ensure a steady state indicated by a plateau. The emission of NBD, the energy donor, was monitored at $530\ \text{nm}$ with the excitation set at $467\ \text{nm}$. Fluorescence intensity before peptide addition was referred to as 0% lipid mixing. In the fusion inhibition experiment, inhibitor peptide solutions of varying con-

centrations were added to the lipid mixture and equilibrated prior to addition of the active peptide solution. 100% lipid mixing was normalized according to 0.03 [peptide:lipid] of N70 in Figure 2, whereas in Figure 8 the activity of each peptide before addition of inhibitor was normalized separately.

Electron microscopy

The effects of the peptides on liposome suspensions were determined by negative stain electron microscopy. Prior to staining and fixing, suspensions of PC:PS:chol LUV at $4\ \text{mM}$ (with or without lyophilized peptide) were incubated for 20 min at room temperature. A drop of the suspension containing PC:PS:chol LUV or a mixture of PC:PS:chol LUV and peptide at a peptide/lipid molar ratio of 0.1 was deposited onto a carbon-coated grid and negatively stained with phosphotungstic acid (2%, pH 6.8). The grids were examined using a JEOL JEM 100B electron microscope (Japan Electron Optics Laboratory Co., Tokyo, Japan). The vesicles' diameters in each image were then compared in a *t*-test to calculate a *p* value.

Preparation of supported lipid bilayers

Supported lipid bilayers were prepared using the vesicle fusion method.⁶⁴ Briefly, PC:PS:chol SUV suspensions ($0.7\ \text{mM}$, $70\ \mu\text{l}$) were deposited onto freshly cleaved mica squares ($1\ \text{cm}^2$) and allowed to adsorb and fuse on the solid surface for 4 h at room temperature followed by rinsing. Samples were then placed in a $1.1\ \text{ml}$ liquid chamber for AFM measurements.

Atomic force microscopy (AFM)

Supported bilayers were investigated using a commercial atomic force microscope (NTEGRA, NT-MDT,

Zelenograd, Russia) equipped with a 100 $\mu\text{m} \times 100 \mu\text{m} \times 5 \mu\text{m}$ Smena scanner. AFM images were obtained in semi-contact mode at room temperature (23–25 °C) in a 1.1 ml liquid cell (MP1LC) filled with either 30 mM NaCl buffer in the case of N36 or with 30 mM NaCl buffer containing 10% DMSO in the case of FP and N70. N36 was dissolved in 30 mM NaCl, while both FP and N70 were dissolved first in DMSO and diluted in 30 mM NaCl to 10% DMSO. Samples were then injected into the liquid chamber to reach 6 μM peptide concentration, and images were taken ~10 min later. All images were recorded using oxide-sharpened microfabricated Si_3N_4 cantilevers (DNP-S, Veeco Metrology LLC, Santa Barbara, CA) with a spring constant of ~0.3 N/m (manufacturer specified) and at a scan rate of 1–1.5 Hz. Large scale images were taken after each scan to assure that changes in membrane morphology were not caused by the tip. Images were obtained from at least two different samples prepared on different days with at least four macroscopically distinct areas on each sample.

Attenuated total reflection-FTIR spectroscopy

Spectra were obtained with a Bruker equinox 55 FTIR spectrometer equipped with a deuterated triglyceride sulfate (DTGS) detector and coupled with an ATR device. For each spectrum, 250 scans were collected with a resolution of 4 cm^{-1} . Samples were prepared as described.⁴⁹ Briefly, lipids alone or with peptide (peptide: lipid molar ratio of 1:180) were deposited on a ZnSe horizontal ATR prism (80 mm \times 7 mm). Previous to sample preparation, the trifluoroacetate (CF_3COO^-) counterions, which associate strongly with the peptide, were replaced with chloride ions through several washings in 0.1 M HCl and lyophilization. This eliminated the strong C=O stretching absorption band near 1673 cm^{-1} .⁶⁵ Peptides were dissolved in MeOH and lipid films in 1:2(v/v) MeOH/ CHCl_3 mixture. Lipid/peptide mixtures or lipids alone with the corresponding volume of methanol were spread with a Teflon bar on the ZnSe prism. Solvents were eliminated by drying under vacuum for 30 min. The background for each spectrum was a clean ZnSe prism. Samples were hydrated by introducing an excess of deuterium oxide ($^2\text{H}_2\text{O}$) into a chamber placed on top of the ZnSe prism in the ATR casting and incubating for up to 60 min, with spectra acquisition every 5 to 10 min. Hydrogen/deuterium exchange was considered complete due to the complete shift of the amide II band. Subtraction of atmospheric H_2O vapor for each sample was carried out as described.⁶⁶ The absorbance of peptide(s) alone was obtained by subtracting the signal of the peptides in lipid from lipid alone (for H_2O corrected spectra), each deuterated for equal time. We processed the subtracted spectra using PEAKFIT (Jandel Scientific, San Rafael, CA) software. For accurate comparison, the absorption of the peptide(s) alone in the amide I (1570–1700 cm^{-1}) was baseline-corrected. Second-derivative spectra were calculated to identify the positions of the component absorption peaks in the spectra. For direct comparison of amide I peptide(s) spectra, the global absorbance intensity was normalized at 1651 cm^{-1} .

Membrane binding

N36 and N36(I62D)m interactions with membranes were analyzed and quantified using fluorescence anisotropy of their intrinsic Trp residues in the presence of phospholipid model membranes at different lipid-to-peptide ratios. Excitation and emission wavelengths

were set to 270/350 nm respectively, and 1 μM of peptide (in 400 μl PBS) was titrated with 5 mM membrane solution successively. As Trp is known to change its emission in hydrophobic environment,⁴⁰ change in its emission represented the amount of peptide bound to membranes. The system reached binding equilibrium (F_{max}) at a certain lipid/peptide ratio allowing calculation of the affinity constant from the relations between the equilibrium level of Trp emission and the lipid concentration (C), using a steady-state affinity model. The affinity constants were then determined by non-linear least squares (NLLSQ). The NLLSQ fitting was done using the following equation:

$$F(x) = \frac{K_a \times X \times F_{\text{max}}}{1 + K_a \times X}$$

where $F(x)$ is the measured Trp fluorescence of the peptide at each lipid concentration X , F_{max} is the maximal fluorescence (it represents the maximum peptide bound to lipids), and K_a is the affinity constant.

N36/C34 core study in membranes

Free Rhodamine labeled peptides were dissolved from lyophilized powder directly in PBS (pH 7.4), to a final concentration of 0.5 μM . Corresponding cores were prepared by dissolving unlabeled counterpart peptide in the solution of labeled peptide to a final concentration of 1 μM unlabeled peptide. By using an excess of unlabeled peptide, we assure that all of the labeled subunits assemble into bundles. Samples were then transferred (400 μl) to glass cuvettes for individual measurements and incubated overnight at room temperature in the dark. Each labeled free peptide and its corresponding core was prepared from a single stock of labeled peptide and measurements were collected intermittently between samples of free peptide and core to control for conditions of sample preparation and incubation time. For fluorescence measurements, equilibrated samples were mixed with magnetic stirring at room temperature and baseline signal was recorded for 2.5 min, whereupon either protease K (10 μl at 2.5 mg/ml for a final concentration of 62.5 $\mu\text{g}/\text{ml}$) or vesicles (20 μl at 18 mM for a final concentration of 900 μM) were added and measurements continued for additional 15 min to follow initial kinetic changes. Next, samples were incubated for 2.5 h in the dark at room temperature to equilibrate following initial treatment. Samples were then measured for 2.5 min to record maximal fluorescence change following incubation with either protease or membrane. For samples in membrane, protease K was then added and fluorescence was recorded for an additional 15 min to follow kinetic change. These samples were then incubated 2.5 h in the dark at room temperature. Maximal change following incubation with both membrane and protease in tandem was then measured for these samples for 2.5 min. Duplicate measurements were collected for each sample from the same stock preparation. To characterize fluorescence changes upon interaction with membranes, a high concentration of vesicles (900 μM) was required to assure maximal binding by peptides and cores.

Acknowledgements

This study was supported in part by the Israel Science Foundation and the Estate of Julius and

Hanna Rosen. Y. S. holds the Harold S. and Harriet B. Brady Professorial Chair in Cancer Research.

References

- Verkleij, A. J., Zwaal, R. F., Roelofsen, B., Comfurius, P., Kastelijn, D. & van Deenen, L. L. (1973). The asymmetric distribution of phospholipids in the human red cell membrane. A combined study using phospholipases and freeze-etch electron microscopy. *Biochim. Biophys. Acta*, **323**, 178–193.
- Virtanen, J. A., Cheng, K. H. & Somerharju, P. (1998). Phospholipid composition of the mammalian red cell membrane can be rationalized by a superlattice model. *Proc. Natl Acad. Sci. USA*, **95**, 4964–4969.
- Fadok, V. A., Voelker, D. R., Campbell, P. A., Cohen, J. J., Bratton, D. L. & Henson, P. M. (1992). Exposure of phosphatidylserine on the surface of apoptotic lymphocytes triggers specific recognition and removal by macrophages. *J. Immunol.* **148**, 2207–2216.
- Bevers, E. M., Comfurius, P., van Rijn, J. L., Hemker, H. C. & Zwaal, R. F. (1982). Generation of prothrombin-converting activity and the exposure of phosphatidylserine at the outer surface of platelets. *Eur. J. Biochem.* **122**, 429–436.
- Driesen, R. B., Dispersyn, G. D., Verheyen, F. K., van den Eijnde, S. M., Hofstra, L., Thone, F. *et al.* (2005). Partial cell fusion: a newly recognized type of communication between dedifferentiating cardiomyocytes and fibroblasts. *Cardiovasc. Res.* **68**, 37–46.
- van den Eijnde, S. M., van den Hoff, M. J., Reutelingsperger, C. P., van Heerde, W. L., Henfling, M. E., Vermeij-Keers, C. *et al.* (2001). Transient expression of phosphatidylserine at cell-cell contact areas is required for myotube formation. *J. Cell Sci.* **114**, 3631–3642.
- Gautier, I., Coppey, J. & Durieux, C. (2003). Early apoptosis-related changes triggered by HSV-1 in individual neuronlike cells. *Exp. Cell Res.* **289**, 174–183.
- Dalgleish, A. G., Beverley, P. C., Clapham, P. R., Crawford, D. H., Greaves, M. F. & Weiss, R. A. (1984). The CD4 (T4) antigen is an essential component of the receptor for the AIDS retrovirus. *Nature*, **312**, 763–767.
- Maddon, P. J., Dalgleish, A. G., McDougal, J. S., Clapham, P. R., Weiss, R. A. & Axel, R. (1986). The T4 gene encodes the AIDS virus receptor and is expressed in the immune system and the brain. *Cell*, **47**, 333–348.
- Jones, P. L., Korte, T. & Blumenthal, R. (1998). Conformational changes in cell surface HIV-1 envelope glycoproteins are triggered by cooperation between cell surface CD4 and co-receptors. *J. Biol. Chem.* **273**, 404–409.
- Feng, Y., Broder, C. C., Kennedy, P. E. & Berger, E. A. (1996). HIV-1 entry cofactor: functional cDNA cloning of a seven-transmembrane, G protein-coupled receptor. *Science*, **272**, 872–877.
- Alkhatib, G., Combadiere, C., Broder, C. C., Feng, Y., Kennedy, P. E., Murphy, P. M. & Berger, E. A. (1996). CC CKR5: a RANTES, MIP-1 α , MIP-1 β receptor as a fusion cofactor for macrophage-tropic HIV-1. *Science*, **272**, 1955–1958.
- Barbouche, R., Miquelis, R., Jones, I. M. & Fenouillet, E. (2003). Protein-disulfide isomerase-mediated reduction of two disulfide bonds of HIV envelope glycoprotein 120 occurs post-CXCR4 binding and is required for fusion. *J. Biol. Chem.* **278**, 3131–3136.
- Veronese, F. D., DeVico, A. L., Copeland, T. D., Oroszlan, S., Gallo, R. C. & Sarngadharan, M. G. (1985). Characterization of gp41 as the transmembrane protein coded by the HTLV-III/LAV envelope gene. *Science*, **229**, 1402–1405.
- Kowalski, M., Potz, J., Basiripour, L., Dorfman, T., Goh, W. C., Terwilliger, E. *et al.* (1987). Functional regions of the envelope glycoprotein of human immunodeficiency virus type 1. *Science*, **237**, 1351–1355.
- Munoz-Barroso, I., Durell, S., Sakaguchi, K., Appella, E. & Blumenthal, R. (1998). Dilution of the human immunodeficiency virus-1 envelope glycoprotein fusion pore revealed by the inhibitory action of a synthetic peptide from gp41. *J. Cell Biol.* **140**, 315–323.
- Chan, D. C., Fass, D., Berger, J. M. & Kim, P. S. (1997). Core structure of gp41 from the HIV envelope glycoprotein. *Cell*, **89**, 263–273.
- Weissenhorn, W., Dessen, A., Harrison, S. C., Skehel, J. J. & Wiley, D. C. (1997). Atomic structure of the ectodomain from HIV-1 gp41. *Nature*, **387**, 426–430.
- Kozlov, M. M., Leikin, S. L., Chernomordik, L. V., Markin, V. S. & Chizmadzhev, Y. A. (1989). Stalk mechanism of vesicle fusion. Intermixing of aqueous contents. *Eur. Biophys. J.* **17**, 121–129.
- Chernomordik, L. V., Melikyan, G. B. & Chizmadzhev, Y. A. (1987). Biomembrane fusion: a new concept derived from model studies using two interacting planar lipid bilayers. *Biochim. Biophys. Acta*, **906**, 309–352.
- LaBranche, C. C., Galasso, G., Moore, J. P., Bolognesi, D. P., Hirsch, M. S. & Hammer, S. M. (2001). HIV fusion and its inhibition. *Antiviral. Res.* **50**, 95–115.
- Eckert, D. M. & Kim, P. S. (2001). Mechanisms of viral membrane fusion and its inhibition. *Annu. Rev. Biochem.* **70**, 777–810.
- Wild, C., Greenwell, T. & Matthews, T. (1993). A synthetic peptide from HIV-1 gp41 is a potent inhibitor of virus-mediated cell-cell fusion. *AIDS Res. Hum. Retroviruses*, **9**, 1051–1053.
- Nieva, J. L., Nir, S., Muga, A., Goni, F. M. & Wilschut, J. (1994). Interaction of the HIV-1 fusion peptide with phospholipid vesicles: different structural requirements for fusion and leakage. *Biochemistry*, **33**, 3201–3209.
- Peisajovich, S. G., Epand, R. F., Pritsker, M., Shai, Y. & Epand, R. M. (2000). The polar region consecutive to the HIV fusion peptide participates in membrane fusion. *Biochemistry*, **39**, 1826–1833.
- Sackett, K. & Shai, Y. (2002). The HIV-1 gp41 N-terminal heptad repeat plays an essential role in membrane fusion. *Biochemistry*, **41**, 4678–4685.
- Pascual, R., Moreno, M. R. & Villalain, J. (2005). A peptide pertaining to the loop segment of human immunodeficiency virus gp41 binds and interacts with model biomembranes: implications for the fusion mechanism. *J. Virol.* **79**, 5142–5152.
- Suarez, T., Nir, S., Goni, F. M., Saez-Cirion, A. & Nieva, J. L. (2000). The pre-transmembrane region of the human immunodeficiency virus type-1 glycoprotein: a novel fusogenic sequence. *FEBS Letters*, **477**, 145–149.
- Shnaper, S., Sackett, K., Gallo, S. A., Blumenthal, R. & Shai, Y. (2004). The C- and the N-terminal regions of glycoprotein 41 ectodomain fuse membranes enriched and not enriched with cholesterol, respectively. *J. Biol. Chem.* **279**, 18526–18534.
- Markosyan, R. M., Cohen, F. S. & Melikyan, G. B. (2003). HIV-1 envelope proteins complete their folding into six-helix bundles immediately after fusion pore formation. *Mol. Biol. Cell*, **14**, 926–938.

31. Dimitrov, A. S., Louis, J. M., Bewley, C. A., Clore, G. M. & Blumenthal, R. (2005). Conformational changes in HIV-1 gp41 in the course of HIV-1 envelope glycoprotein-mediated fusion and inactivation. *Biochemistry*, **44**, 12471–12479.
32. Hamburger, A. E., Kim, S., Welch, B. D. & Kay, M. S. (2005). Steric accessibility of the HIV-1 gp41 N-trimer region. *J. Biol. Chem.* **280**, 12567–12572.
33. Kliger, Y., Peisajovich, S. G., Blumenthal, R. & Shai, Y. (2000). Membrane-induced conformational change during the activation of HIV-1 gp41. *J. Mol. Biol.* **301**, 905–914.
34. Rabenstein, M. & Shin, Y. K. (1995). A peptide from the heptad repeat of human immunodeficiency virus gp41 shows both membrane binding and coiled-coil formation. *Biochemistry*, **34**, 13390–13397.
35. Kliger, Y., Aharoni, A., Rapaport, D., Jones, P., Blumenthal, R. & Shai, Y. (1997). Fusion peptides derived from the HIV type 1 glycoprotein 41 associate within phospholipid membranes and inhibit cell-cell Fusion. Structure-function study. *J. Biol. Chem.* **272**, 13496–13505.
36. Dubay, J. W., Roberts, S. J., Brody, B. & Hunter, E. (1992). Mutations in the leucine zipper of the human immunodeficiency virus type 1 transmembrane glycoprotein affect fusion and infectivity. *J. Virol.* **66**, 4748–4756.
37. Pascual, R., Contreras, M., Fedorov, A., Prieto, M. & Villalain, J. (2005). Interaction of a peptide derived from the N-heptad repeat region of gp41 Env ectodomain with model membranes. Modulation of phospholipid phase behavior. *Biochemistry*, **44**, 14275–14288.
38. Deshayes, S., Plenat, T., Aldrian-Herrada, G., Divita, G., Le Grimellec, C. & Heitz, F. (2004). Primary amphipathic cell-penetrating peptides: structural requirements and interactions with model membranes. *Biochemistry*, **43**, 7698–7706.
39. Sackett, K. & Shai, Y. (2005). The HIV fusion peptide adopts intermolecular parallel beta-sheet structure in membranes when stabilized by the adjacent N-terminal heptad repeat: a 13C FTIR study. *J. Mol. Biol.* **350**, 790–805.
40. Jameson, D. M. & Sawyer, W. H. (1995). Fluorescence anisotropy applied to biomolecular interactions. *Methods Enzymol.* **246**, 283–300.
41. Lu, M. & Kim, P. S. (1997). A trimeric structural subdomain of the HIV-1 transmembrane glycoprotein. *J. Biomol. Struct. Dynam.* **15**, 465–471.
42. Epand, R. M., Shai, Y., Segrest, J. P. & Anantharamaiah, G. M. (1995). Mechanisms for the modulation of membrane bilayer properties by amphipathic helical peptides. *Biopolymers*, **37**, 319–338.
43. Wexler-Cohen, Y., Sackett, K. & Shai, Y. (2005). The role of the N-terminal heptad repeat of HIV-1 in the actual lipid mixing step as revealed by its substitution with distant coiled coils. *Biochemistry*, **44**, 5853–5861.
44. Gordon, L. M., Curtain, C. C., Zhong, Y. C., Kirkpatrick, A., Mobley, P. W. & Waring, A. J. (1992). The amino-terminal peptide of HIV-1 glycoprotein 41 interacts with human erythrocyte membranes: peptide conformation, orientation and aggregation. *Biochim. Biophys. Acta*, **1139**, 257–274.
45. Martin, I., Defrise-Quertain, F., Decroly, E., Vandendriessche, M., Brasseur, R. & Ruysschaert, J. M. (1993). Orientation and structure of the NH2-terminal HIV-1 gp41 peptide in fused and aggregated liposomes. *Biochim. Biophys. Acta*, **1145**, 124–133.
46. Rafalski, M., Lear, J. D. & DeGrado, W. F. (1990). Phospholipid interactions of synthetic peptides representing the N-terminus of HIV gp41. *Biochemistry*, **29**, 7917–7922.
47. Pereira, F. B., Goni, F. M., Muga, A. & Nieva, J. L. (1997). Permeabilization and fusion of uncharged lipid vesicles induced by the HIV-1 fusion peptide adopting an extended conformation: dose and sequence effects. *Biophys. J.* **73**, 1977–1986.
48. Yang, J., Gabrys, C. M. & Weliky, D. P. (2001). Solid-state nuclear magnetic resonance evidence for an extended beta strand conformation of the membrane-bound HIV-1 fusion peptide. *Biochemistry*, **40**, 8126–81237.
49. Sackett, K. & Shai, Y. (2003). How structure correlates to function for membrane associated HIV-1 gp41 constructs corresponding to the N-terminal half of the ectodomain. *J. Mol. Biol.* **333**, 47–58.
50. Arispe, N. (2004). Architecture of the Alzheimer's A beta P ion channel pore. *J. Membr. Biol.* **197**, 33–48.
51. Arispe, N., Pollard, H. B. & Rojas, E. (1993). Giant multilevel cation channels formed by Alzheimer disease amyloid beta-protein [A beta P-(1-40)] in bilayer membranes. *Proc. Natl Acad. Sci. USA*, **90**, 10573–10577.
52. Thundimadathil, J., Roeske, R. W., Jiang, H. Y. & Guo, L. (2005). Aggregation and porin-like channel activity of a beta sheet peptide. *Biochemistry*, **44**, 10259–10270.
53. Wild, C. T., Shugars, D. C., Greenwell, T. K., McDanal, C. B. & Matthews, T. J. (1994). Peptides corresponding to a predictive alpha-helical domain of human immunodeficiency virus type 1 gp41 are potent inhibitors of virus infection. *Proc. Natl Acad. Sci. USA*, **91**, 9770–9774.
54. Jiang, S., Lin, K., Strick, N. & Neurath, A. R. (1993). HIV-1 inhibition by a peptide. *Nature*, **365**, 113.
55. Pombourios, P., Wilson, K. A., Center, R. J., El Ahmar, W. & Kemp, B. E. (1997). Human immunodeficiency virus type 1 envelope glycoprotein oligomerization requires the gp41 amphipathic alpha-helical/leucine zipper-like sequence. *J. Virol.* **71**, 2041–2049.
56. Wild, C., Dubay, J. W., Greenwell, T., Baird, T., Jr, Oas, T. G., McDanal, C. *et al.* (1994). Propensity for a leucine zipper-like domain of human immunodeficiency virus type 1 gp41 to form oligomers correlates with a role in virus-induced fusion rather than assembly of the glycoprotein complex. *Proc. Natl Acad. Sci. USA*, **91**, 12676–12680.
57. Chen, S. S., Lee, C. N., Lee, W. R., McIntosh, K. & Lee, T. H. (1993). Mutational analysis of the leucine zipper-like motif of the human immunodeficiency virus type 1 envelope transmembrane glycoprotein. *J. Virol.* **67**, 3615–3619.
58. Chen, S. S. (1994). Functional role of the zipper motif region of human immunodeficiency virus type 1 transmembrane protein gp41. *J. Virol.* **68**, 2002–2010.
59. Dimitrov, A. S., Xiao, X., Dimitrov, D. S. & Blumenthal, R. (2001). Early intermediates in HIV-1 envelope glycoprotein-mediated fusion triggered by CD4 and co-receptor complexes. *J. Biol. Chem.* **276**, 30335–30341.
60. Merrifield, R. B., Vizioli, L. D. & Boman, H. G. (1982). Synthesis of the antibacterial peptide cecropin A (1-33). *Biochemistry*, **21**, 5020–5031.
61. Shai, Y., Bach, D. & Yanovsky, A. (1990). Channel formation properties of synthetic pardaxin and analogues. *J. Biol. Chem.* **265**, 20202–20209.
62. Rapaport, D. & Shai, Y. (1991). Interaction of fluorescently labeled pardaxin and its analogues with lipid bilayers. *J. Biol. Chem.* **266**, 23769–23775.
63. Struck, D. K., Hoekstra, D. & Pagano, R. E. (1981). Use of resonance energy transfer to monitor membrane fusion. *Biochemistry*, **20**, 4093–4099.

64. Yang, T., Simanek, E. E. & Cremer, P. (2000). Creating addressable aqueous microcompartments above solid supported phospholipid bilayers using lithographically patterned poly(dimethylsiloxane) molds. *Anal. Chem.* **72**, 2587–2589.
65. Surewicz, W. K., Mantsch, H. H. & Chapman, D. (1993). Determination of protein secondary structure by Fourier transform infrared spectroscopy: a critical assessment. *Biochemistry*, **32**, 389–394.
66. Vigano, C., Goormaghtigh, E. & Ruyschaert, J. M. (2003). Detection of structural and functional asymmetries in P-glycoprotein by combining mutagenesis and H/D exchange measurements. *Chem. Phys. Lipids*, **122**, 121–135.
67. Sackett, K., Wexler-Cohen, Y. & Shai, Y. (2006). Characterization of the HIV N-terminal fusion peptide containing region in context of key gp41 fusion conformations. *J. Biol. Chem.* **281**, 21755–21762.

Edited by J. Karn

(Received 5 July 2006; received in revised form 31 August 2006; accepted 31 August 2006)
Available online 5 September 2006